OXFORD Toxicology Research

Toxicology Research, 2022, **11**, 42–51
https://doi.org/10.1093/toxres/tfab105
Advance access publication date 8 December 2021
Paper

SiO_2-induced ferroptosis in macrophages promotes the development of pulmonary fibrosis in silicosis models

Taiyang Liu[1,2], Rui Bao[1,2], Qiushi Wang[1,2], Wei Hao[1,2], Yaoyang Liu[1,2], Sirong Chang[1,2], Meng Wang[1,2], Yuanyuan Li[1,2], Zhihong Liu[1,2,†,*], Yue Sun[1,2,†,*]

[1]School of Public Health and Management, Ningxia Medical University, No. 1160, Shengli Street, Xingqing District, Yinchuan 75000, Ningxia, China,
[2]NHC KEY Laboratory of Metabolic Cardiovascular Diseases Research, Ningxia Medical University, No. 1160, Shengli Street, Xingqing District, Yinchuan 75000, Ningxia, China

*Correspondence address. School of Public Health and Management, Ningxia Medical University, No. 1160, Shengli Street, Xingqing District, Yinchuan 75000, Ningxia, China. Tel: +023-722-305-61; E-mail: zhihongliu2021@163.com; liuzhihong@nxmu.edu.cn; 781002564@qq.com

†These authors contributed equally to this work.

Silicosis is a devastating disease that, without effective treatment, endangers the health of miners. Therefore, studies exploring the pathogenesis of SiO_2-induced pulmonary fibrosis are necessary to develop treatments for silicosis. Although macrophages are known to play a pivotal role in SiO_2-induced pulmonary fibrosis, the underlying mechanism remains unknown. Here, we explored whether ferroptosis was involved in SiO_2-induced pulmonary fibrosis. To this end, C57BL/6 mice and mouse macrophage (RAW264.7) cells and mouse lung fibroblast (MLF) cells were subjected to iron content, cell viability, enzyme-linked immunosorbent assay, immunofluorescence staining, histological, western blotting, quantitative reverse transcription-PCR, reactive oxygen species, and lipid peroxidation analysis. *In vivo*, SiO_2 was found to damage the lung alveolar structure, cause infiltration of inflammatory cells, and facilitate fibrosis. Additionally, it increased the iron concentration and lipid peroxidation as well as altered the expression of ferroptosis-related genes and the mitochondrial morphology in macrophages. *In vitro*, ferroptosis occurred in SiO_2-treated RAW264.7 cells, which showed iron overload, lipid peroxidation, and gene alterations. Furthermore, ferrostatin-1 (Fer-1) attenuated ferroptosis in SiO_2-treated RAW264.7 cells by inhibiting lipid peroxidation and cell death and regulating ferroptosis-related genes expression, in addition to attenuating the secretion of pro-fibrotic cytokines and fibrosis. Collectively, SiO_2 induces ferroptosis in macrophages, which leads to the secretion of pro-fibrotic cytokines and fibrosis.

Key words: silicosis; macrophage; ferroptosis; ferrostatin-1; lipid peroxidation.

Introduction

Silicosis is a serious occupational disease that endangers the health of workers worldwide [1] and is characterized by persistent pulmonary fibrosis. A study conducted in 2015 showed that the incidence of silicosis is relatively high in South Africa [2] as well as in India where 11.5 million workers were reported to be exposed to silica dust [3]. Patients with silicosis have respiratory and circulatory dysfunction accompanied by cough, sputum, chest tightness, dyspnea, chest pain, and fatigue. Treatment approaches include pulmonary lavage and antifibrosis drugs; although these treatments inhibit fibrosis development during silicosis, they fail to remove residual SiO_2 in the alveolar cavity. Therefore, exploring the pathogenesis of SiO_2-induced pulmonary fibrosis is necessary for developing treatments.

Macrophages have a pivotal role in the pathogenesis of SiO_2-induced pulmonary fibrosis by secreting various pro-fibrotic cytokines in response to SiO_2 [4]. Therefore, macrophages damage or death may initiate SiO_2-induced pulmonary fibrosis. In the pathogenesis of SiO_2-induced pulmonary fibrosis, macrophages damage or death occur through programmed cell death (PCD) processes such as apoptosis, autophagy, and pyroptosis. Apoptosis plays a significant role in the progression of silicosis. SiO_2 binding to the scavenger receptor on the alveolar macrophage surface can trigger the upregulation of FasL, which binds Fas and leads to apoptosis. Additionally, autophagy regulates the synthesis and degradation of cellular components and plays a pivotal part in the pathogenesis of silicosis. SiO_2 is found in the macrophage autophagolysosomes of patients with silicosis, and unusual autophagy activity has been observed in rats with silicosis [5, 6]. In addition, pyroptosis accompanied by rupture of the nuclear DNA and cell membrane leads to the release of a large number of inflammatory factors (such as interleukin (IL)-α, IL-1β, and IL-33) [7]. However, the pathogenesis of pulmonary fibrosis remains controversial. It was previously reported that after the inhibition of special damage or death types, pulmonary fibrosis was not significantly attenuated [8]. It indicates that other mechanisms may be involved in SiO_2-induced pulmonary fibrosis.

Received: August 9, 2021. **Revised:** October 12, 2021. **Accepted:** October 18, 2021

Ferroptosis is a type of PCD discovered in 2012. The iron-mediated Fenton reaction induces reactive oxygen species (ROS) and lipid peroxidation, which causes cell membrane disruption, including mitochondria, and results in ferroptosis [9]. Studies have shown that ferroptosis occurs in various pulmonary diseases. Cigarette smoke promotes iron overload and phospholipid peroxidation, leading to ferroptosis in chronic obstructive pulmonary disease [10]. ROS accumulation and glutathione (GSH) depletion, which are closely associated with ferroptosis, strongly affect the pathogenesis of pulmonary diseases [11]. Additionally, Li observes that irradiation induces ROS and changes the concentration of inflammatory cytokines. Ferroptotic characteristic changes of mitochondria in acute radiation-induced lung injury (RILI) was observed by transmission electron microscopy (TEM). In summary, ferroptosis participates in RILI [12, 13]. Nevertheless, the role of ferroptosis in SiO_2-induced pulmonary fibrosis remains unclear. Here, we explored the role of ferroptosis in SiO_2-induced pulmonary fibrosis and the underlying mechanisms.

Materials and Methods

Mouse models

C57BL/6 mice (22 ± 2 g) were purchased from the Ning Xia Medical University Laboratory Animal Centre and fed in a sterile environment. The animal procedures were approved by the Ethics Committee of Ningxia Medical University (approval no. 2020-493). Mice were randomly assigned to the SiO_2 group, which was treated with 100 μl SiO_2 suspensions (100 mg/ml) via intratracheal instillation, or saline group as controls. The animals were anesthetized with isoflurane and sacrificed after 56 days.

Cell culture and SiO_2 treatment

The RAW264.7 cells (mouse macrophage, MINGJIN BIOLOGY, Shanghai, China) and the MLF cells (mouse lung fibroblast, Procell Life Science&Technology Co., Ltd, Wuhan, China) cultured in Dulbecco's modified Eagle medium (Gibco, Grand Island, NY, USA) supplemented with 10% fetal bovine serum (Gibco) in an incubator with 5% CO_2 at 37°C. The SiO_2 group was treated with 50 $\mu g/cm^2$ SiO_2 suspension for 24 h. The saline group was treated with saline. Ferrostatin-1 (Fer-1, 10 μM, a ferroptosis inhibitor, Selleck, Houston, USA) or Z-VAD-FMK (20 μM, a caspase inhibitor that inhibits apoptosis, Selleck, Houston, USA) was added to the RAW264.7 cells 1 h before SiO_2 administration.

Coculture experiment

We used a 24 mm Transwell® (Corning, NY, USA). RAW264.7 cells were seeded into the upper wells and treated with SiO_2 (50 $\mu g/cm^2$) for 24 h. Fer-1 (10 μM) was added to the RAW264.7 1 h before SiO_2 administration. MLF cells attached to the lower wells were cocultured with RAW264.7 cells in a Transwell 6-wells plate system for another 24 h. The supernatant was collected for cytokine detection, and MLF cells were collected to detect the protein and mRNA levels of α-smooth muscle actin (α-sma), matrix metalloprotein-9 (MMP-9), and collagen-1.

GSH/GSSG assay and MDA assay

The glutathione/glutathione oxidized (GSH/GSSG) and malondialdehyde (MDA) levels were measured using a GSH/GSSG assay kit (Nanjing Jiancheng Bioengineering Institute, Nanjing, China) and MDA assay kit (BestBio, Shanghai, China), respectively, as per the manufacturer's instructions.

Iron assay

Iron concentrations in the lung tissues and cells were measured using an iron assay kit (Nanjing Jiancheng Bioengineering Institute, Nanjing, China) and iron colorimetric assay kit (Applygen Technologies, Beijing, China), respectively, as per the manufacturer's instructions.

Cell viability assay

Cell viability was assessed using Cell Counting Kit-8 (Beyotime Biotechnology, Shanghai, China) as per the manufacturer's instructions. Cell viability% = Absorbance of (experimental group-blank control group)/absorbance of (control group-blank control group) × 100%.

ROS measurement

Briefly, ROS levels were assessed using the dichlorodihydro-fluorescein diacetate (DCFH-DA) probe (BestBio, Shanghai, China). RAW264.7 cells were cultured in 35 mm confocal dishes and exposed to an SiO_2 suspension (50 $\mu g/cm^2$) for 24 h. The DCFH-DA probe (1:1000) was added to the cells and incubated for 20 min, followed by three washes with phosphate-buffered saline (PBS). Fluorescence intensity was observed via laser scanning confocal microscopy.

Lipid peroxidation measurement

Lipid peroxidation was measured using the C11-BODIPY$^{581/591}$ probe (Thermo Fisher Scientific, Waltham, MA, USA). Upon ROS-induced intracellular lipid peroxidation, the fluorescent signal of this probe shifts from red to green. The fluorescent signal was detected using laser scanning confocal microscopy (LSM800, Carl Zeiss, Jena, Germany). RAW264.7 cells were incubated for 20–30 min with C11-BODIPY$^{581/591}$ (1 μM) in a confocal dish. The fluorescence of the probe was measured by simultaneous acquisition of the red (Texas red) and green (fluorescein isothiocyanate) signals.

Immunofluorescence staining

Frozen lung tissue sections or cells were fixed in 4% paraformaldehyde for 25 min at room temperature, washed with PBS for 15 min, permeabilized for 20 min with 0.3% Triton X-100, and blocked for 1 h with 1% bovine serum albumin. Anti-XCT antibody (1:100, #ab37185, Abcam, Cambridge, UK) and anti-

GPX_4 antibody (1:100, #ab125066, Abcam, Cambridge, UK) were incubated with the sections for 1–2 h at room temperature. The nucleus was labeled using 4′,6-diamidino-2-phenylindole (DAPI). Fluorescent images were acquired via laser scanning confocal microscopy (LSM800, Carl Zeiss, Jena, Germany).

Histology

After fixation in 4% paraformaldehyde, lung tissues were embedded in paraffin and cut into 6-μm-thick paraffin sections. The sections were stained with hematoxylin and eosin (H&E) to visualize silicosis nodules and Sirius red and Masson to visualize fibrosis. The procedures were conducted according to the manufacturer's instructions.

Transmission electron microscopy

The lung tissues were fixed with 2.5% glutaraldehyde and 1% osmium tetroxide and cut into 60–70 nm-thick sections. After staining with uranyl acetate and lead citrate, mitochondrial morphological features were observed via TEM (JEOL, Tokyo, Japan).

Enzyme-linked immunosorbent assay

The levels of interleukin-1β (IL-1β), tumor necrosis factor-α (TNF-α), and transforming growth factor-β (TGF-β) in the supernatant were analyzed using enzyme-linked immunosorbent assay kits according to the manufacturer's instructions (JONLN Reagent Co., Ltd, Shanghai, China). The absorbance was detected at 450 nm.

Western blotting

The lung tissue homogenates and cells were ground using a grinder. Total protein was extracted using the Whole Cell Lysis Assay Kit (KeyGEN BioTECH, Nanjing, China). Proteins were separated via 10%–12% sodium dodecyl sulfate-polyacrylamide gel electrophoresis and then transferred to polyvinylidene fluoride membranes. The membranes were blocked in 5% skim milk at room temperature for 2 h and washed six times (5 min each) with PBS containing Tween 20. Next, the membranes were incubated with anti-XCT (1:1000, #ab37185, Abcam, Cambridge, UK), anti-GPX_4 (1:1000, #ab125066, Abcam, Cambridge, UK), anti-α-SMA antibody (1:1000, #AF1032, Affinity Biosciences, Jiangsu, China), anti-MMP-9 antibody (1:1000, #ab38898, Abcam, Cambridge, UK), anti-collagen-1 antibody (1:1000, #ab260043, Abcam, Cambridge, UK), and anti-β-actin antibody (1:5000, #SC-47778, Santa Cruz Biotechnology, Heidelberg, Germany) antibodies for 1–2 h at 37°C or overnight at 4°C, followed by washing with PBS containing Tween 20 and incubation with a goat antirabbit secondary antibody (1:5000, ZSGB-BIO, Beijing, China) at room temperature for 2–4 h. The membranes were incubated with enhanced chemiluminescence solution for 5 s to visualize the protein bands.

Quantitative reverse transcription-polymerase chain reaction

Total RNA was extracted from the lung homogenates and cell lysates using the RNA simple Total RNA Kit (TIANGEN, Beijing, China). RNA quality was detected using SimpliNano (GE Healthcare, Little Chalfont, UK). PrimeScript RT Master Mix (TaKaRa, Shiga, Japan) was used for the reverse transcription of RNA into cDNA, and then quantitative reverse transcription-polymerase chain reaction (qRT-PCR) was performed using TB Green Premix Ex Taq II (TaKaRa, Shiga, Japan) according to the manufacturer's instructions. The cycling conditions were as follows: 30 s at 95°C followed by 40 cycles of 95°C for 5 s and 60°C for 30 s. The following qRT-PCR primers were used: GPX_4: forward, 5′-TGTGCATCCCGCGATGATT-3′, reverse, 5′-CCCTGTACTTATCCAGGCAGA-3′; XCT: forward: 5′-GGCACCGTCATCGGATCAG-3′, reverse, 5′-CTCCACAGGCAGACCAGAAAA-3′;GAPDH: forward, 5′-AGGTCGGTGTGAACGGATTTG-3′, reverse, 5′-GGGGTCGT TGATGGCAACA-3′. The cycle threshold (Ct) values were acquired, and the relative expression of *XCT* and *GPX_4* was calculated using the $2^{-\Delta\Delta Ct}$ method. *GAPDH* was used as an internal control. All experiments were performed in triplicates.

Statistical analysis

All statistical analyses and visualization of graphs were performed using the GraphPad 8 software (GraphPad, Inc., La Jolla, CA, USA). Data are shown as mean ± standard deviation. Comparisons between two groups were performed using Student's *t*-test. Multiple groups were analyzed using one-way analysis of variance followed by Tukey's multiple comparisons test. $P < 0.05$ was considered to indicate statistically significant results.

Results

SiO_2 promoted lung injury and fibrosis in mice

H&E staining revealed that SiO_2 injured the normal structure, thickened the alveolar wall, and caused infiltration of inflammatory cells in the lungs. Silicosis nodules were detected in SiO_2-induced lung tissues, whereas no significant histological changes were observed in the saline group (Fig. 1A). Masson and Sirius red staining were performed to observe lung fibrosis. Compared to that in the saline group, collagen deposition obviously increased in the SiO_2 group (Fig. 1B and C). α-sma and collagen-1 expression are related to lung fibrosis, and western blot analysis revealed that SiO_2 upregulated the expression of these proteins (Fig. 1D and E). qRT-PCR analysis showed that the mRNA levels of α-sma and collagen-1 were markedly increased (Fig. 1F and G). Collectively, SiO_2 facilitated lung injury and fibrosis in mice.

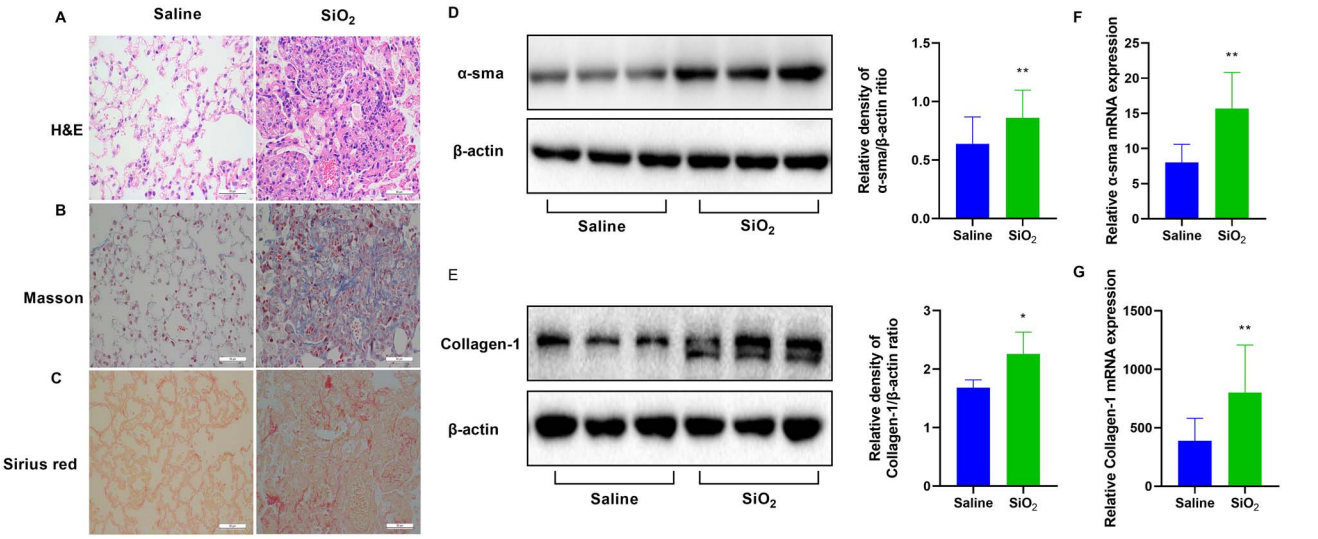

Figure 1. SiO_2 promotes lung injury and fibrosis in mice. To induce lung injury and fibrosis, mice were intratracheally injected with SiO_2 (100 mg/ml). Representative images of (A) hematoxylin and eosin (H&E) staining, (B) Masson staining, and (C) Sirius red staining of the lung tissue sections. Scale bars, 50 μm. Western blotting and quantification of the (D) α-smooth muscle actin (α-sma) and (E) collagen-1 proteins in the indicated groups. mRNA expression of (F) α-sma and (G) collagen-1 in the indicated groups. *$P < 0.05$ vs. saline group; **$P < 0.01$ vs. saline group.

Ferroptosis occurred in mice after treatment with SiO_2

Next, we examined whether ferroptosis occurred in SiO_2-treated mice. Iron is necessary for ferroptosis for inducing the Fenton reaction. Thus, ferroptosis is largely characterized by excessive iron levels. SiO_2 increased iron concentration in the SiO_2-treated group (Fig. 2A). Lipid peroxidation is a well-known biomarker of ferroptosis. MDA is an important endogenous metabolite of lipid peroxidation. We estimated MDA levels in the lung tissues using the MDA assay kit and immunofluorescence. As shown in Figure 2B and C, MDA levels were increased in the SiO_2 group. GSH and GSSG are characteristic markers of ferroptosis. We observed that the GSH/GSSG ratio was decreased in SiO_2-treated mice (Fig. 2D). Based on the importance of GPX_4 and XCT in the regulation of ferroptosis, we measured the protein and mRNA expression of these molecules in mice. GPX_4 expression was decreased and XCT expression was increased in SiO_2-treated mice (Fig. 2E–H). Ferroptosis is known to cause typical changes in the mitochondrial morphology by reducing cristae, and rupturing the outer membrane. To identify which cell types involved in ferroptosis, we scanned all cell types with TEM in the lungs of mice. Compared to that in the saline group, we observed reduced numbers of cristae, and a ruptured outer membrane in macrophages from the SiO_2-treated lung tissues (Fig. 2I). These results indicated that ferroptosis occurred in macrophages. Therefore, we focused ferroptosis in macrophages in further experiments.

Ferroptosis was observed in SiO_2-treated RAW264.7 cells

To examine whether SiO_2-induced ferroptosis occurred *in vitro*, we used mouse macrophages RAW264.7. Cell viability showed that the number of dead RAW264.7 cells was higher in the SiO_2-treated group than in the saline group (Fig. 3A). Iron concentration increased in the SiO_2 group (Fig. 3B). ROS and lipid peroxidation, which are well-known biomarkers of ferroptosis, were measured in RAW264.7 cells after SiO_2 treatment using a DCFH-DA probe, MDA, GSH/GSSG, and the C11-BODIPY$^{581/591}$ assay kit. MDA concentration was increased and the GSH/GSSG ratio was decreased in SiO_2-treated cells (Fig. 3C and D). The number of positive cells stained by DCFH-DA probe was increased in the SiO_2 group (Fig. 3E). The number of unoxidized positive cells stained with C11-BODIPY$^{581/591}$ was decreased, whereas that of oxidized positive cells was increased after treatment with SiO_2 (Fig. 3F), indicated increased lipid peroxidation. Additionally, GPX_4 expression was decreased and XCT expression was increased in SiO_2-treated cells (Fig. 3G–L). These findings indicated that SiO_2 stimulated ferroptosis in RAW264.7 cells.

Fer-1 protected against oxidative stress and attenuated ferroptosis in RAW264.7 cells, whereas Z-VAD-FMK did not

Fer-1 is a classic ferroptosis inhibitor and Z-VAD-FMK is a classic apoptosis inhibitor. The number of dead cells was remarkably decreased in the SiO_2 + Fer-1 group, which was not affected by Z-VAD-FMK treatment (Fig. 4A). MDA concentration was increased in SiO_2-treated RAW264.7 cells and was attenuated in Fer-1-treated cells; However, Z-VAD-FMK caused no significant change (Fig. 4B). The GSH/GSSG ratio, recovered after Fer-1 treatment but not after Z-VAD-FMK treatment (Fig. 4C). ROS levels were reduced in the presence of Fer-1, but not in the presence of Z-VAD-FMK (Fig. 4D). Lipid peroxidation was reduced in RAW264.7 cells pretreated with Fer-1, whereas Z-VAD-FMK had no effect (Fig. 4E). Fer-1 treatment, but not Z-VAD-FMK treatment, significantly increased the

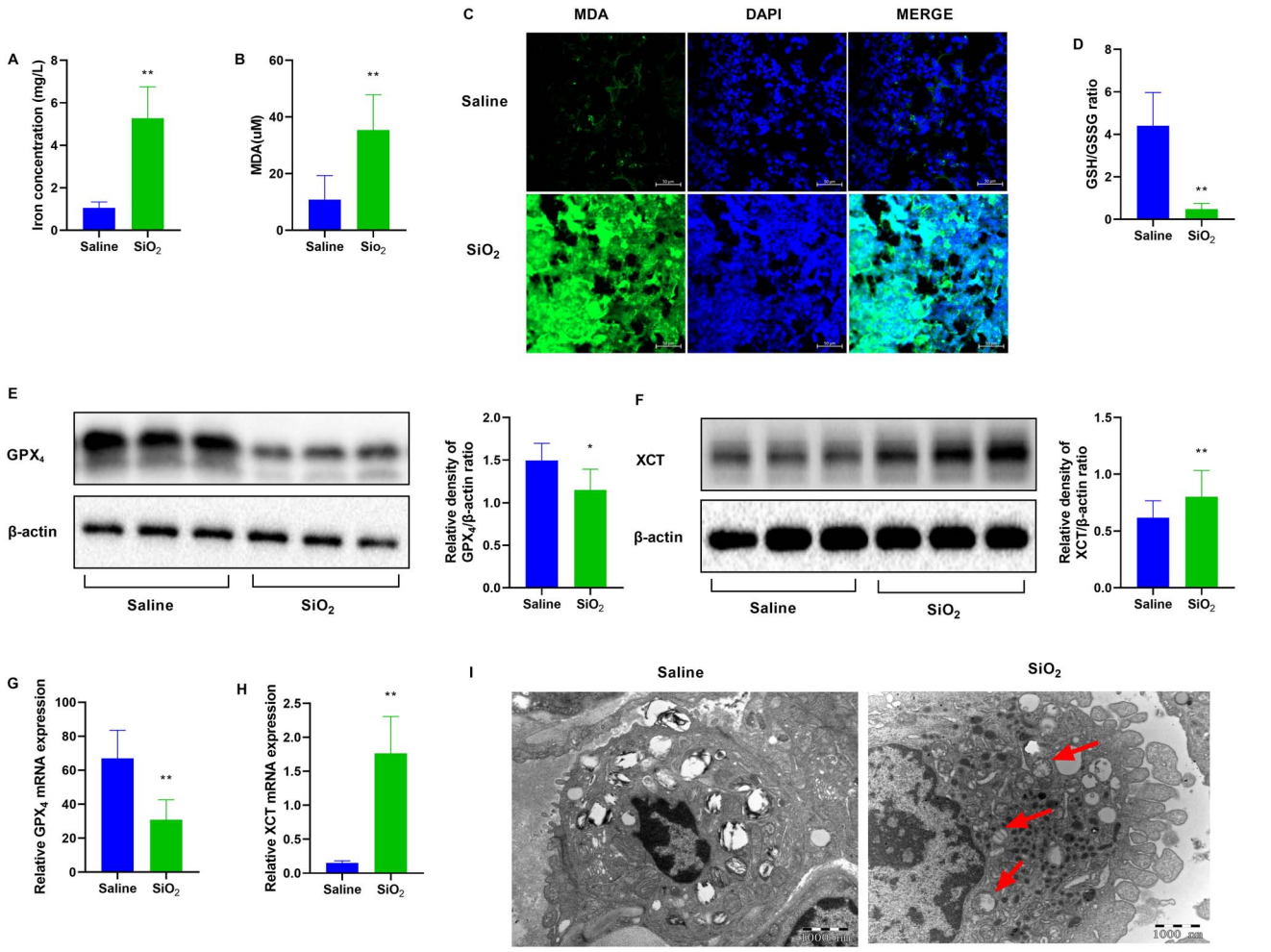

Figure 2. SiO_2 induces ferroptosis in mice. Mice were intratracheally injected with SiO_2 (100 mg/ml) for 56 days. $n = 6$ per group. (A) Iron concentration in the lung tissue sections from the indicated groups. (B) Malondialdehyde (MDA) levels for peroxide formation and (C) MDA staining. Scale bars, 50 μm. (D) The glutathione/glutathione oxidized (GSH/GSSG) assay. Western blotting and quantification of the (E) GPX_4 and (F) XCT proteins in lung tissues from saline and SiO_2 groups. mRNA expression of (G) GPX_4 and (H) XCT in lung tissues from mice exposed to saline or SiO_2. (I) Mitochondrial morphological changes were detected via transmission electron microscopy (TEM). Typical mitochondrial morphology in ferroptosis is indicated with red arrows. Scale bars, 1000 nm. *$P < 0.05$ vs. saline group; **$P < 0.01$ vs. saline group.

expression of GPX_4 and downregulated that of XCT (Fig. 4F–I). However, Fer-1 was not found to regulate iron concentration. The function of Fer-1 may not depend on iron metabolism while regulating lipid peroxidation. These datas suggested that ferroptosis occurred in SiO_2-treated RAW264.7 cells, and that Fer-1 protected against oxidative stress and attenuated ferroptosis in RAW264.7 cells, whereas Z-VAD-FMK did not.

Fer-1 alleviated SiO_2-induced fibrosis *in vitro*

Fibroblasts act as effector cells of pulmonary fibrosis by secreting extracellular matrix proteins. Thus, we examined fibroblasts *in vitro*. We established a coculture system with RAW264.7 cells (mouse macrophage) and MLF cells (mouse lung fibroblast) (Fig. 5A), and the supernatant and MLF cells were collected. IL-1β, TNF-α, and TGF-β are critical pro-fibrotic cytokines. The results of enzyme-linked immunosorbent assay (ELISA) showed that Fer-1 effectively inhibited the secretion of pro-fibrotic cytokines in the supernatant (Fig. 5B–D). Furthermore, we measured the expression of α-sma, collagen-1, and MMP-9 in MLF cells. Western blot analysis showed that the expression of α-sma, collagen-1, and MMP-9 was decreased by Fer-1 (Fig. 5E), which is consistent with the qRT-PCR data (Fig. 5F–H). These findings indicated that Fer-1 might alleviate fibrosis in MLF cells by inhibiting ferroptosis in SiO_2-treated RAW264.7 cells, which secreted pro-fibrotic cytokines.

Discussion

In vivo, we found that SiO_2 damaged the alveolar structure, caused infiltration of inflammatory cells, and facilitated fibrosis. SiO_2 increased the iron concentration and lipid peroxidation and altered the expression of ferroptosis-related genes, such as GPX_4 and XCT, and the mitochondrial morphology in macrophages. These results indicated that ferroptosis occurred in macrophages. *In vitro*, we observed that ferroptosis occurred in SiO_2-treated RAW264.7 cells, which showed

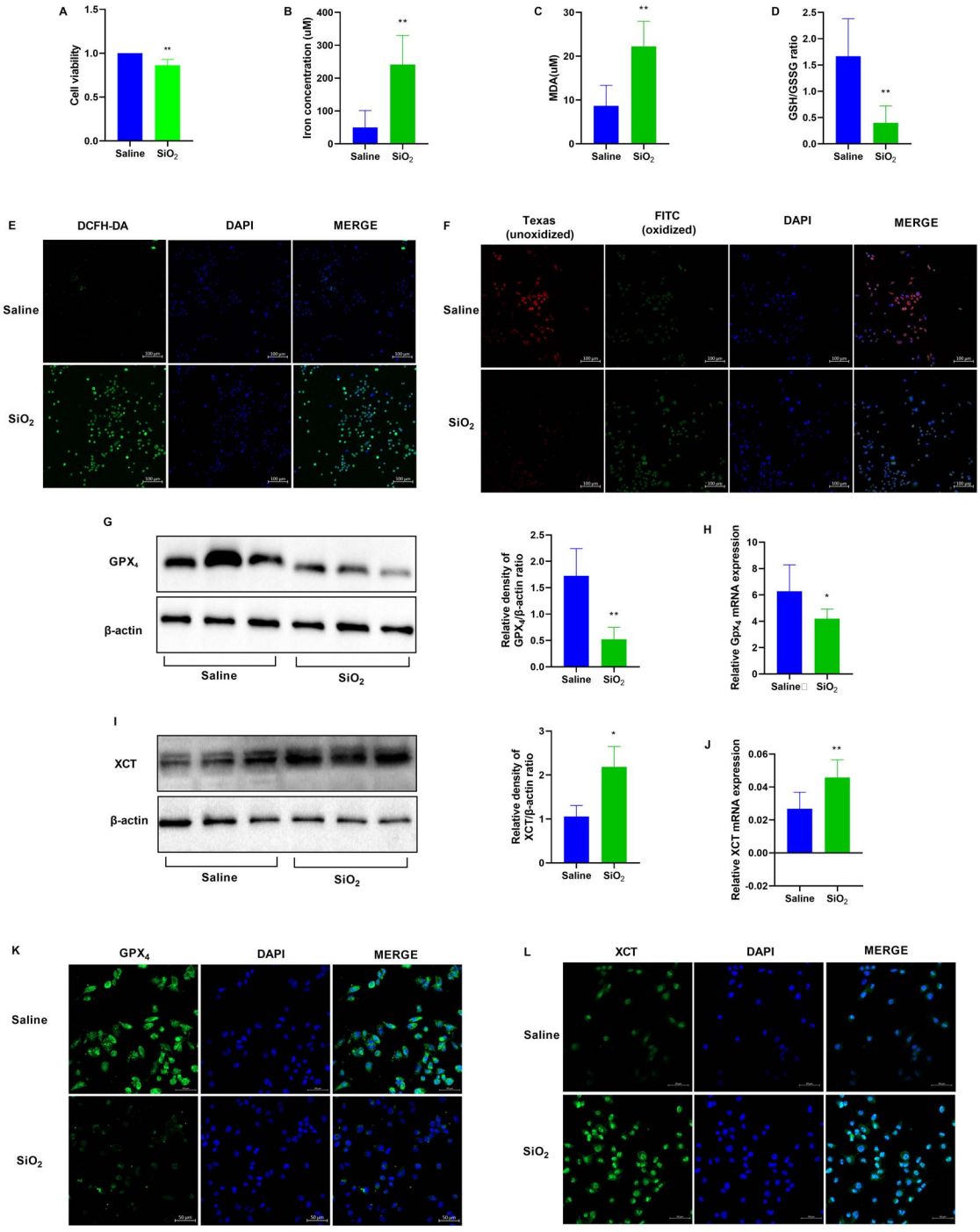

Figure 3. SiO_2 induces ferroptosis in RAW264.7 cells. RAW264.7 cells were treated with saline or SiO_2 suspension at 50 $\mu g/cm^2$ for 24 h. $n = 3$ per group. (A) Cell viability of RAW264.7 cells detected with CCK-8 assay. (B) Iron concentration in RAW264.7 cells in the indicated groups. (C) Malondialdehyde (MDA) levels and (D) The glutathione/glutathione oxidized (GSH/GSSG) assay. (E) Reactive oxygen species (ROS) was observed using DCFH-DA. Scale bars, 100 μm. (F) Lipid peroxidation was measured using the C11-BODIPY$^{581/591}$ probe. Scale bars, 100 μm. Western blotting and quantification of the (G) GPX_4 and (I) XCT proteins in RAW264.7 cells in the saline and SiO_2 groups. mRNA expression of (H) GPX_4 and (J) XCT in RAW264.7 cells in the saline and SiO_2 groups. Representative images of RAW264.7 cells showing the expression of (K) GPX_4 and (L) XCT. Scale bars, 50 μm. $^*P < 0.05$ vs. saline group; $^{**}P < 0.01$ vs. saline group.

iron overload, lipid peroxidation, and gene expression alterations. In addition, Fer-1 attenuated ferroptosis in SiO_2-treated RAW264.7 cells by inhibiting lipid peroxidation and cell death and suppressing the expression of ferroptosis-related genes. Furthermore, Fer-1 alleviated fibrosis in MLF cells by inhibiting the ferroptosis in SiO_2-treated RAW264.7 cells that secreted pro-fibrotic cytokines. Taken together, SiO_2 induced ferroptosis in macrophages that secreted pro-fibrotic cytokines and resulted in fibrosis.

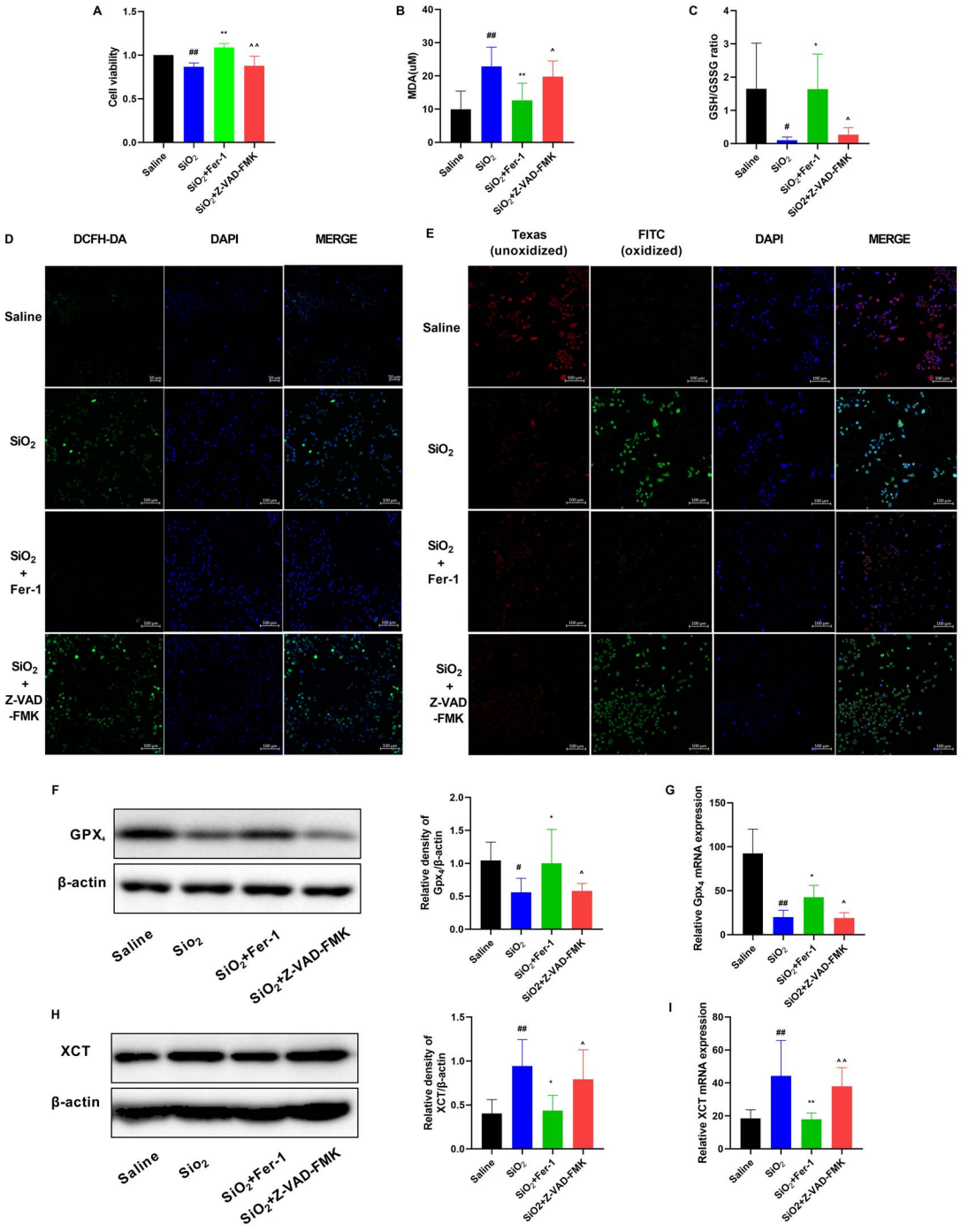

Figure 4. Fer-1 protects against oxidative stress and attenuates ferroptosis in RAW264.7 cells. RAW264.7 cells were treated with saline or an SiO_2 suspension at 50 $\mu g/cm^2$ for 24 h. Fer-1 (10 μM) or Z-VAD-FMK (20 μM) was added to RAW264.7 cells 1 h before SiO_2 administration. (A) Cell viability of RAW264.7 cells detected with CCK-8 assay. (B) Malondialdehyde (MDA) levels and (C) The glutathione/glutathione oxidized (GSH/GSSG) assay. (D) ROS was observed using DCFH-DA probe. Scale bars, 100 μm. (E) Lipid peroxidation was measured using the C11-BODIPY$^{581/591}$ probe. Scale bars, 100 μm. Western blotting and quantification of the (F) GPX_4 and (H) XCT proteins in the indicated groups. mRNA expression of (G) GPX_4 and (I) XCT in the indicated groups. #$P < 0.05$ vs. saline group; ##$P < 0.01$ vs. saline group. *$P < 0.05$ vs. SiO_2 group; **$P < 0.01$ vs. SiO_2 group. ^$P < 0.05$ vs. SiO_2 + Fer-1 group; ^^$P < 0.01$ vs. SiO_2 + Fer-1 group.

Iron overload can accelerate the accumulation of lipid peroxides, which depends on the Fenton reaction, and influences ferroptosis sensitivity [14]. Ferroptosis requires transferrin and the transferrin receptor to import iron from the extracellular environment [15]. Knocking out the key gene of iron metabolism, iron responsive element binding protein 2 (IREB2), has been reported to decrease ferroptosis [9]. In our study, SiO_2 upregulated iron concentration to trigger ferroptosis in SiO_2-induced pulmonary fibrosis. Ferroptosis is also

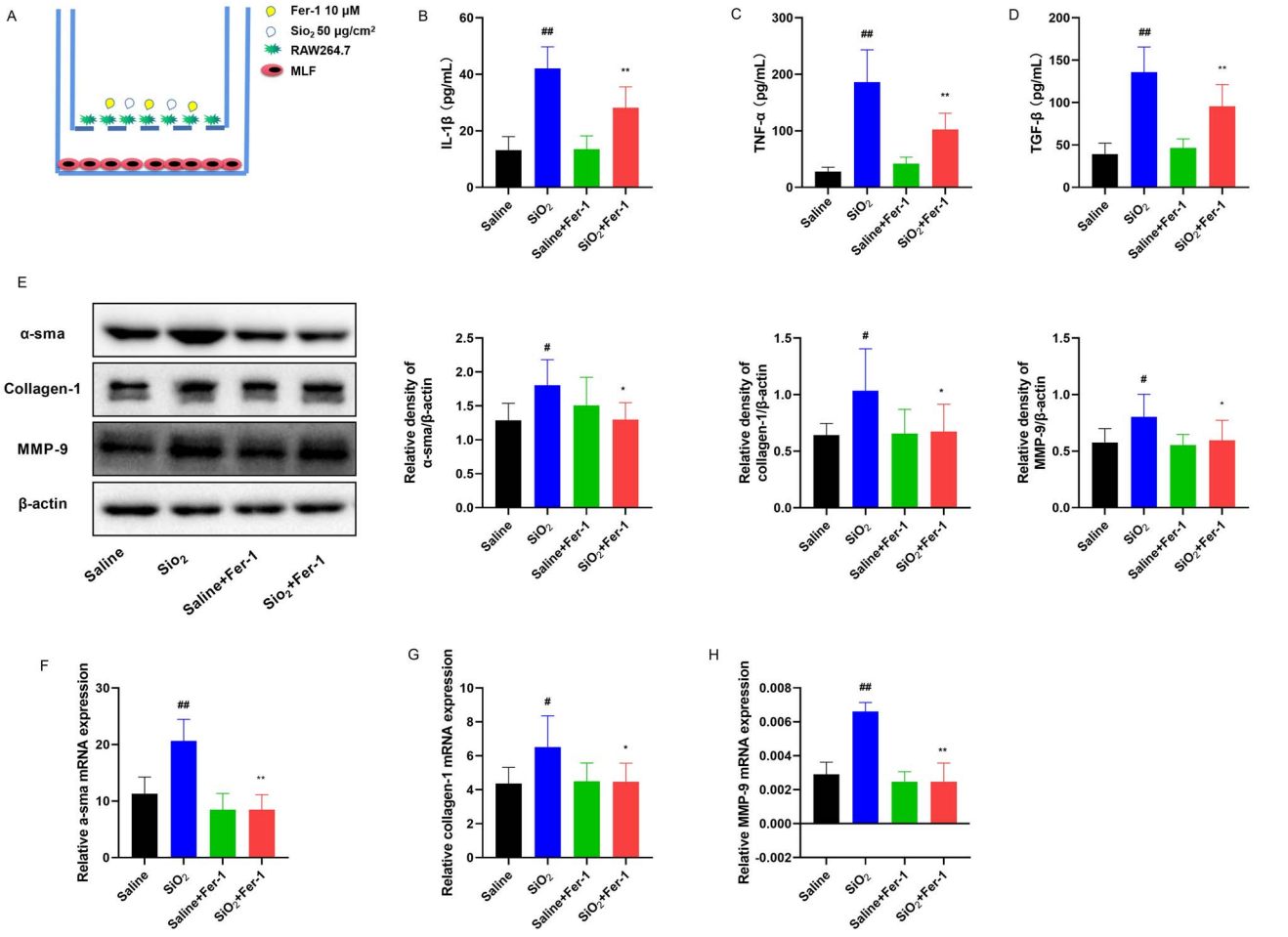

Figure 5. Fer-1 alleviates SiO_2-induced fibrosis *in vitro*. RAW264.7 cells seeded into the upper wells were treated with SiO_2 (50 $\mu g/cm^2$) for 24 h. Fer-1 (10 μM) was added to RAW264.7 cells 1 h before SiO_2 administration. MLF cells attached to the lower wells were cocultured with RAW264.7 cells in a Transwell 6-wells plate system for another 24 h. The supernatant was collected to detect cytokines, and MLF cells were collected to detect the protein and mRNA levels of α-sma, collagen-1, and MMP-9. $n = 3$ per group. (A) The coculture system of RAW264.7 cells and MLF cells. Levels of (B) IL-β, (C) TNF-α, and (D) TGF-β were measured in the supernatant by ELISA after 24 h of coculture. (E) Western blotting and quantification of the α-sma, collagen-1, and MMP-9 proteins in the indicated group. mRNA expression of (F) α-sma, (G) collagen-1, and (H) MMP-9 in the indicated group. #$P < 0.05$ vs. saline group; ##$P < 0.01$ vs. saline group. *$P < 0.05$ vs. SiO_2 group; **$P < 0.01$ vs. SiO_2 group.

defined as a form of regulated cell death, which is induced by lipid peroxidation. We predicted that SiO_2 induces iron overload and triggers ROS production via the Fenton reaction, leading to lipid peroxidation and ferroptosis development. Taken together, both iron overload and lipid peroxidation greatly affect ferroptosis in SiO_2-induced pulmonary fibrosis.

GPX_4 and XCT are the main proteins involved in ferroptosis. GPX_4 is a selenoprotein glutathione peroxidase [16]. Silencing of GPX_4 increases embryonic mortality in postcoitum, with concomitantly increased cell death. GPX_4 has been identified as a key regulator of ferroptosis [17–19]. In this study, GPX_4 expression was reduced in SiO_2-induced models. In agreement with previous findings, the reduced expression of GPX_4 was found to induce ferroptosis. XCT imports cystine and exports glutamate simultaneously to supply glutathione that attenuates oxidative stress. Inhibition of XCT can result in GSH depletion and ferroptosis [20]. Interestingly, we observed increased expression of XCT after treatment with SiO_2 *in vivo* and *in vitro*, contrasting the results of previous studies. SiO_2 may stimulate a negative feedback mechanism to suppress ferroptosis via the rapid consumption of GSH. Moreover, the function of XCT is unclear, although it is known to be related to ferroptosis, but silencing of the XCT gene cannot trigger ferroptosis *in vivo* [21]. Possibly, SiO_2-induced models may initiate a protective mode against ferroptosis by increasing the expression of XCT. Altogether, SiO_2 regulates GPX_4 and XCT, suggesting that ferroptosis is involved in SiO_2-induced pulmonary fibrosis.

Fer-1 is a synthetic compound that inhibits ferroptosis and generally accepted hydroperoxyl radicals as a scavenger. *In vitro*, by scavenging lipid peroxides, Fer-1 can inhibit ferroptosis. In this study, Fer-1 significantly attenuated the SiO_2-induced MDA content, GSH/GSSG, ROS, and lipid peroxidation and inhibited SiO_2-induced cell death. Furthermore, Fer-1 alleviated fibrosis in MLF cells by inhibiting the ferroptosis of SiO_2-treated RAW264.7 cells that secreted pro-fibrotic cytokines. These results

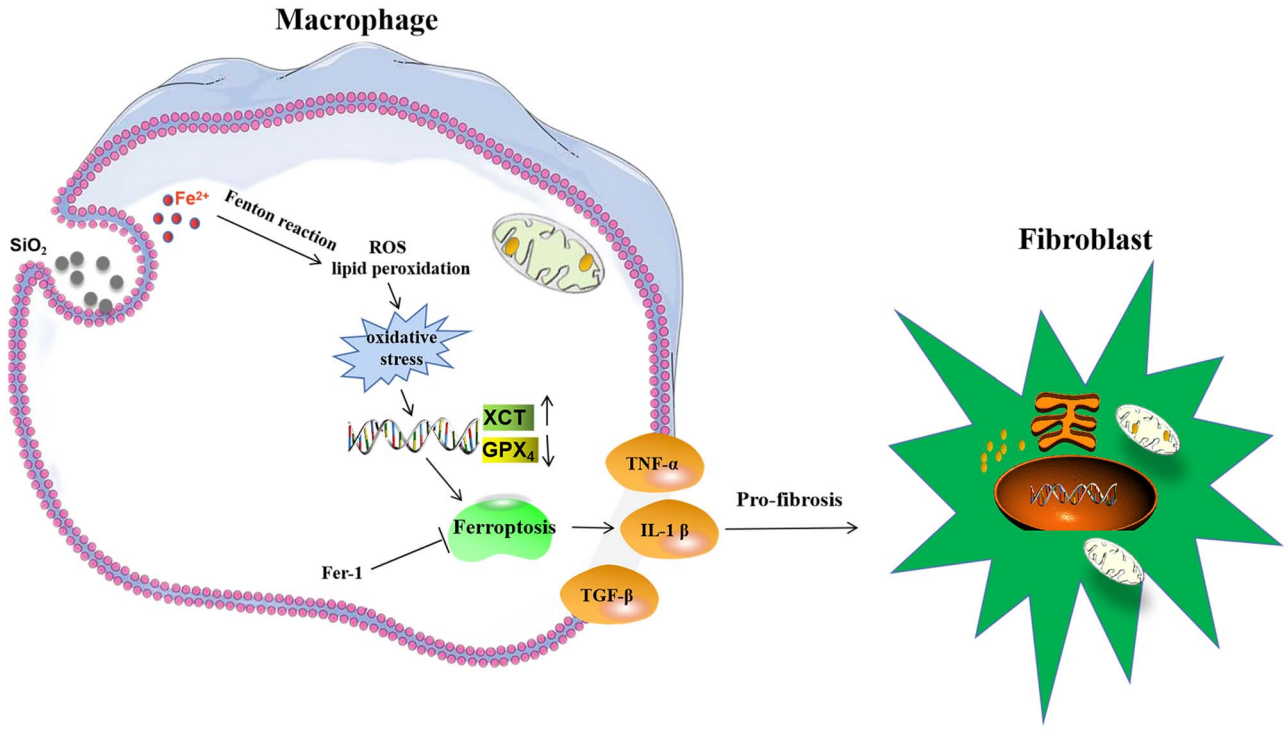

Figure 6. Summary illustration showing a relationship between SiO_2-induced ferroptosis in macrophages and pulmonary fibrosis.

suggest that SiO_2 induces ferroptosis in SiO_2-induced pulmonary fibrosis.

Our study has many limitations; for example, the causes of increased iron concentration and alterations of ferroptosis-related genes are unclear. Additionally, the precise mechanism of how SiO_2 induces ferroptosis in silicosis must be determined. Our further studies will focus on pathways regulating ferroptosis-related genes.

Conclusions

In this study, after macrophages engulfed SiO_2, SiO_2 increased the intracellular iron levels, which induced ROS and lipid peroxidation through the Fenton reaction. After the exhaustion of GSH, oxidative stress was increased, which might regulate ferroptosis-related genes, eventually resulting in ferroptosis. Ferroptotic macrophages secreting pro-fibrotic cytokines initiated the fibrosis process through an interaction with fibroblasts (Fig. 6). In conclusion, our findings indicate that SiO_2-induced ferroptosis in macrophages promotes the development of pulmonary fibrosis in silicosis models.

Authors' contributions

Zhihong Liu designed the current study. Rui Bao participated in data collection and organization. Taiyang Liu and Yue Sun wrote the manuscript together. Qiushi Wang, Wei Hao, Yaoyang Liu, Sirong Chang, Meng Wang, and Yuanyuan Li performed the statistical analysis and made critical comments. The author(s) read and approved the final manuscript.

Conflicts of Interest Statement

The authors declare that they have no competing interests.

Acknowledgments

This research was funded by the National Natural Science Foundation of China grant numbers 81960018 and 82060264, Science and Technology Department of Ningxia grant number 2020BEG03008, and Ningxia Medical University Scientific Research Project grant number XT2018012. We are thankful to Ningxia Medical University for funding this work. We would like to thank Editage (www.editage.cn) for English language editing.

References

1. Sitong D, Li C, Yiping L *et al.* Dioscin alleviates crystalline silica-induced pulmonary inflammation and fibrosis through promoting alveolar macrophage autophagy. *Theranostics* 2019;**9**:1878–92.
2. Knight D, Ehrlich R, Fielding K *et al.* Trends in silicosis prevalence and the healthy worker effect among gold miners in South Africa: a prevalence study with follow up of employment status. *BMC Public Health* 2015;**15**:1258–67.
3. Jindal SK. Silicosis in India: past and present. *Curr Opin Pulm Med* 2013;**19**:163–8.
4. Song L, Weng D, Dai W *et al.* Th17 can regulate silica-induced lung inflammation through an IL-1beta-dependent mechanism. *J Cell Mol Med* 2014;**18**:1773–84.
5. du Bois RM. Strategies for treating idiopathic pulmonary fibrosis. *Nat Rev Drug Discov* 2010;**9**:129–40.

6. Wang M, Jin Y, Chen S *et al.* The study of autophagy in alveolar macrophages of patients with coal workers' pneumoconiosis. *Zhonghua Lao Dong Wei Sheng Zhi Ye Bing Za Zhi* 2015;**33**:41–4.
7. Chen S, Jin Y-L, Yao S-Q *et al.* Autophagy in lung tissue of rats exposed to silica dust. *Zhonghua Lao Dong Wei Sheng Zhi Ye Bing Za Zhi* 2013;**31**:607–10.
8. Stegmann KA, De Souza JB, Riley EM. IL-18-induced expression of high-affinity IL-2R on murine NK cells is essential for NK-cell IFN-gamma production during murine Plasmodium yoelii infection. *Eur J Immunol* 2015;**45**:3431–40.
9. Dixon SJ, Lemberg KM, Lemprecht MR *et al.* Ferroptosis: an iron-dependent form of nonapoptotic cell death. *Cell* 2012;**149**:1060–72.
10. Yoshida M, Minagawa S, Araya J *et al.* Involvement of cigarette smoke-induced epithelial cell ferroptosis in COPD pathogenesis. *Nat Commun* 2019;**10**:3145–59.
11. Wang Y, Tang M. PM2.5 induces ferroptosis in human endothelial cells through iron overload and redox imbalance. *Environ Pollut* 2019;**254**:112937–47.
12. Li X, Zhuang X, Qiao T. Role of ferroptosis in the process of acute radiation-induced lung injury in mice. *Biochem Biophys Res Commun* 2019;**519**:240–5.
13. Li X, Duan L, Yuan S *et al.* Ferroptosis inhibitor alleviates radiation-induced lung fibrosis (RILF) via down-regulation of TGF-β1. *J Inflamm (Lond)* 2019;**16**:11–20.
14. Stockwell BR, Angeli JPF, Bayir H *et al.* Ferroptosis: a regulated cell death nexus linking metabolism, redox biology, and disease. *Cell* 2017;**171**:273–85.
15. Gao M, Monian P, Quadri N *et al.* Glutaminolysis and transferrin regulate ferroptosis. *Mol Cell* 2015;**59**:298–308.
16. Imai H, Matsuoka M, Kumagai T *et al.* Lipid peroxidation-dependent cell death regulated by GPx4 and ferroptosis. *Curr Top Microbiol Immunol* 2017;**403**:143–70.
17. Sakai O, Uchida T, Imai H, Ueta T. Glutathione peroxidase 4 plays an important role in oxidative homeostasis and wound repair in corneal epithelial cells. *FEBS Open Bio* 2016;**6**:1238–47.
18. Sakai O, Uchida T, Roggia MF *et al.* Role of glutathione peroxidase 4 in glutamate-induced oxytosis in the retina. *PLoS One* 2015;**10**:e0130467.
19. Imai H, Hirao F, Sakamoto T *et al.* Early embryonic lethality caused by targeted disruption of the mouse PHGPx gene. *Biochem Biophys Res Commun* 2003;**305**:278–86.
20. Jiang L, Kon N, Li T *et al.* Ferroptosis as a p53-mediated activity during tumor suppression. *Nature* 2015;**520**:57–62.
21. Wang H, An P, Xie E *et al.* Characterization of ferroptosis in murine models of hemochromatosis. *Hepatology* 2017;**66**:449–65.